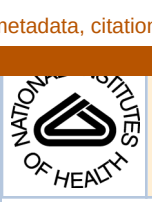



Published in final edited form as:

*Nitric Oxide*. 2012 October 15; 27(3): 161–168. doi:10.1016/j.niox.2012.06.004.

# A system for exposing molecules and cells to biologically relevant and accurately controlled steady-state concentrations of nitric oxide and oxygen

**Vasileios Dendroulakis**[a], **Brandon S. Russell**[b], **C. Eric Elmquist**[b,1], **Laura J. Trudel**[b], **Gerald N. Wogan**[b,c], **William M. Deen**[a,*], and **Peter C. Dedon**[b,c,*]

[a]Department of Chemical Engineering, Massachusetts Institute of Technology, Cambridge, MA 02139, USA

[b]Department of Biological Engineering, Massachusetts Institute of Technology, Cambridge, MA 02139, USA

[c]Center for Environmental Health Sciences, Massachusetts Institute of Technology, Cambridge, MA 02139, USA

## Abstract

Nitric oxide (NO) plays key roles in cell signaling and physiology, with diverse functions mediated by NO concentrations varying over three orders-of-magnitude. In spite of this critical concentration dependence, current approaches to NO delivery in vitro result in biologically irrelevant and poorly controlled levels, with hyperoxic conditions imposed by ambient air. To solve these problems, we developed a system for controlled delivery of NO and $O_2$ over large concentration ranges to mimic biological conditions. Here we describe the fabrication, operation and calibration of the delivery system. We then describe applications for delivery of NO and $O_2$ into cell culture media, with a comparison of experimental results and predictions from mass transfer models that predict the steady-state levels of various NO-derived reactive species. We also determined that components of culture media do not affect the steady-state levels of NO or $O_2$ in the device. This system provides critical control of NO delivery for in vitro models of NO biology and chemistry.

## 1. Introduction

Nitric oxide (NO) is a free-radical gas involved in diverse biological processes, such as apoptosis, neurotransmission, blood pressure control and innate immunity [1]. Of critical importance to NO function is its steady-state concentration in tissues, with biologically relevant concentrations ranging over three orders-of-magnitude. On the basis of literature



*Corresponding authors: PCD, Department of Biological Engineering, 56-787B, Massachusetts Institute of Technology, 77 Massachusetts Avenue, Cambridge, MA 02139; tel: +1 617 253 8017; pcdedon@mit.edu; WMD, Department of Chemical Engineering, 66-572, Massachusetts Institute of Technology, 77 Massachusetts Avenue, Cambridge, MA 02139; tel: +1 617 253 4535; wmdeen@mit.edu.

[1]Present address: Compliant Therapeutics, LLC, 114 Spencer Creed Road, Franklin, TN 37069



**AUTHOR CONTRIBUTIONS** P.C.D., W.M.D., G.N.W., V.D. designed experiments; V.D., B.S.R., C.E.E., L.J.T. performed experiments; V.D., B.S.R., C.E.E., L.J.T., P.C.D., W.M.D., G.N.W. interpreted data and contributed to the writing of the manuscript.

estimates, Thomas et al. proposed concentration categories for NO function, ranging from cGMP-mediated signaling processes at ~1–30 nM, modulation of kinase and transcription factor activity at ~30–400 nM (e.g., Akt, HIF-1α, p53) and pathological nitrosative and oxidative stresses above ~500 nM [2]. The balance between low and high concentrations may thus dictate cell decision-making processes such as survival and proliferation as opposed to growth arrest and cell death. While the functions of NO are controlled in part by the rate of generation by NO synthases, numerous chemical reactions affect its concentration by consuming NO, such as reactions with superoxide ($O_2^{\cdot-}$) to form peroxynitrite ($ONOO^-$), and with molecular oxygen to form the oxidizing and S-nitrosating nitrogen dioxide radical ($NO_2^{\bullet}$) and the S- and N-nitrosating species, nitrous anhydride ($N_2O_3$). Glutathione and other cellular reductants and electrophiles further intervene in reactions with these NO derivatives (e.g., ref. [3]). Activated macrophages are the major source of pathologically high levels of NO [4], producing local steady-state concentrations approaching 1 μM [5]. Simultaneous generation of $O_2^{\cdot-}$ leads to $ONOO^-$, while reactions of NO with $O_2$ yield $N_2O_3$ and $NO_2^{\bullet}$. These reactive species damage all types of cellular biomolecules and thus contribute to the mechanistic link between inflammation and cancer [5,6].

Evidence for the concentration-dependence of NO function highlights the need for delivery of predictable and biologically relevant steady-state levels of NO and $O_2$ in vitro to mimic the biological environment. NO can be introduced into a solution by several methods. One approach to NO delivery in vitro involves the use of “NONOates” that release NO with predictable kinetics to provide transient, non-uniform levels that must be averaged over time to define exposure [7]. Garthwaite and coworkers were able to obtain constant steady-state levels of NO over several minutes by balancing NO release from a NONOate with consumption by a scavenger [8]. The difficulty of controlling the steady-state concentration of NO with NONOates over longer periods of exposure [7,9] is compounded by the unknown effects of the chemical species generated upon release of NO [7], the generation of nitroxyl [10], and the fact that different NO-donor compounds with different half-lives must be used to span a range of exposure times [11]. Alternative methods of NO delivery include addition of aliquots of NO-saturated aqueous solutions, which produce local NO “hotspots” [12], and co-culture of NO-producing macrophages with target cells, which involves poor control of NO levels and complicates interpretation of results with multiple cell lines [13,14].

Over the past decade, we have developed NO delivery systems for controlled steady-state concentrations of NO (0.1–1 μM) and $O_2$ (50–200 μM) to mimic biological environments such as inflammation [15,16]. The best characterized and most widely applicable of the systems employs NO- and $O_2$-permeable polydimethylsiloxane (Silastic) tubing to deliver the gases at constant and predictable levels. Mass transfer models were developed to calculate the concentrations of NO and $O_2$ in the bulk liquid, given any combination of tubing length and gas feed composition [16], as well as rates of gas consumption by cells [17]. The device was designed primarily for cultured cells and was used to elucidate threshold effects in NO-induced toxicity and mutagenicity in human cells [17,18]. However, the mass transfer model was validated only for NO and $O_2$ delivery in phosphate buffers and was not tested with the more complex case of cell culture media, components of which could consume NO, such as riboflavin-generated superoxide that may react with NO [19,20]. Although partial oxidation of NO within the permeable Silastic tubing motivated the development of a Teflon-membrane delivery apparatus for chemical kinetic experiments [21], the Silastic tubing system has proven utility for long-term cell culture studies [16,22].

Here we describe the fabrication of the NO/$O_2$ delivery system from commercially available components, and the operation and calibration of the system. We then describe an application of the system for delivery of NO and $O_2$ into cell culture media, with a

comparison of experimental results with a mass transfer model that predicts the steady-state levels of various NO-derived reactive species. We also determined that photo-sensitive reactions taking place in cell culture media, such as riboflavin-derived $O_2^{\cdot -}$ synthesis, do not affect steady-state NO or $O_2$ levels. Finally, we illustrate use of the delivery system with different cell types and explore the range of cumulative NO-dosing and its effect on cell survival. This system provides critical control of NO delivery for in vitro models of NO biology and chemistry and offers great potential for exploring reactions between nitrogen oxides and biomolecules or cellular components.

## 2. Materials and methods

### 2.1. Fabrication of the delivery system

The $NO/O_2$ delivery system consists of three major components: a vessel for exposing cells (the delivery apparatus), a system for delivering NO and $O_2$ to the exposure vessel (the peripheral tubing system) and accessories for temperature control and stirring. As shown in Figure 1, the delivery apparatus is comprised of a Teflon screw-capped jar with a lid fitted with luer adapters for connecting external gas tubing to the internal Silastic tubing for diffusion of gases into solution, as described previously [16]. The lid can also be modified with ports for probes to monitor solution levels of NO and $O_2$ (Supplementary Figure S1). An alternative configuration was conceived for exposure of adherent cells (Supplementary Figure S2). Gases are delivered at controlled flow rates by the peripheral tubing system (Supplementary Figure S3), which consists of gas tanks, tubing and flow controllers to deliver two gas mixtures to the delivery apparatus: NO in argon (pure argon for controls) and $O_2$ in a mixture of $N_2$ and $CO_2$. Supplementary Tables S1 and S2 contain a complete parts list required to fabricate the system (assembly procedure described in Supplementary Text S1). Temperature control is achieved by immersing the vessel in a water bath mounted on a magnetic stirrer (set at 100 rpm). To avoid operator exposure to NO gas, the system must be operated in a fume hood (Supplementary Figure S4 and Text S3). Gas leak alarms can be installed in the vicinity to minimize the potential for accidental exposure (available online:
http://www.certifiedairsafety.com/bw-technologies-gas-detectors-honewellgasalertmax-gaslaertmicro5/bw-technologies-by-honeywell-gasalert-extreme).

### 2.2. Dissolved NO and $O_2$ measurement in the apparatus

Levels of NO and $O_2$ in the bulk liquid were measured using a modified apparatus where a stainless steel fitting (Swagelok; Supplementary Table S2) was threaded through a drilled hole centered on the device's cap to firmly suspend a dissolved $O_2$ meter Orion 810 A-plus (Thermo Electron). A female luer bulkhead fitting (Cole-Parmer) with its barbed hose filed away and its inner diameter increased to ~4 mm was threaded in a different hole drilled in the cap (Supplementary Figure S1); appropriately sized rubber gaskets (McMaster-Carr) were placed between the fittings and the cap to seal the connections. The 4 mm margin was large enough to allow insertion of the 2 mm ISO-NOP Nitric Oxide probe (World Precision Instruments, Inc.) without disturbing its tip membrane. A rubber gasket that when fitted on the probe exceeded a 4 mm diameter was used to securely immobilize it on the filed luer adapter. To minimize the risk of touching the membrane and destabilizing the signal, the NO electrode remained semi-permanently attached; the $O_2$ probe on the other hand was robust enough to be inserted anew before each exposure. After sealing the container, the tips from both electrodes were immersed in the liquid and protected from any movement or contact with the stirring bar.

### 2.3. Calibration of NO and $O_2$ probes

Both NO and $O_2$ probes were pre-calibrated daily before use. NO electrode calibration involved immersing the tip of the probe in 0.1 M potassium iodide and 0.1 M sulfuric acid while known amounts of a potassium nitrite standard solution were added to the solution, generating an equimolar amount of NO [23]. Linear calibration curves were obtained over the range of 0–2 μM at both 23 and 37 °C. The calibration procedure for the $O_2$ electrode entailed water-saturated air according to the manufacturer's instructions; the probe operated in a range of concentrations of dissolved $O_2$ between 100 and 300 μM.

### 2.4. Exposure of water, RPMI-1640 and DMEM to NO and $O_2$

Two loops of Silastic tubing (Dow Corning; Supplementary Table S2) were attached to the female barbed hose luer fittings fixed on the modified apparatus (Figure 1C), one for NO and the other for $O_2$ (corresponding lengths in Table 1). After pre-calibration, both electrodes were attached and the apparatus was filled with ~115–120 mL of either de-ionized water, RPMI-1640 or DMEM cell medium (BioWhittaker - Lonza). The device was sealed and placed in the water bath at 23 or 37 (± 1) °C. Simultaneous initiation of gas flows followed (procedure described in Supplementary Text S2), employing a 10% NO in argon mixture and a 50% $O_2$:45% $N_2$:5% $CO_2$ mixture (Airgas). Exposures lasted for 40–50 min and experiments were repeated at least 3 times.

### 2.5. Nitrite measurements

For exposures involving pure water, nitrite ($NO_2^-$) concentration was monitored by UV absorbance at 210 nm ($\varepsilon = 5200\ M^{-1}\ cm^{-1}$) [24] in 100 μL samples withdrawn from the device at regular intervals.

### 2.6. NO aqueous oxidation reaction scheme and mass transfer model

In aqueous media at physiological pH, NO reacts with oxygen giving rise to the stable end product nitrite ($NO_2^-$), as illustrated by the following reactions:

$$2NO + O_2 \xrightarrow{k_1} 2NO_2 \quad (1)$$

$$NO + NO_2 \underset{k_{-2}}{\overset{k_2}{\rightleftarrows}} N_2O_3 \quad (2)$$

$$N_2O_3 + H_2O \xrightarrow{k_3} 2NO_2^- + 2H^+ \quad (3)$$

When NO is the only nitrogen oxide added to the system, intermediates $NO_2$ and $N_2O_3$ are present only in trace quantities [25], justifying pseudo-steady state approximations for their concentrations, while the rate-limiting step is Equation (1). In that case, Equations (1), (2) and (3) can simply be combined into the overall reaction:

$$4NO + O_2 + H_2O \xrightarrow{k_1} 4NO_2^- + 4H^+ \quad (4)$$

Employing those approximations to eliminate the concentrations ($C_j$) of the intermediate species as independent variables from the volumetric rate of formation ($R_j$) for species $j$ = NO, $O_2$ and $NO_2^-$ gives, according to Equation (4):

$$R_{NO} = -4k_1 C_{NO}^2 C_{O_2}$$

$$R_{O_2} = -k_1 C_{NO}^2 C_{O_2}$$

$$R_{NO_2^-} = 4k_1 C_{NO}^2 C_{O_2}$$

The mass balance equations for NO, $O_2$and $NO_2^-$, the dominant species during a typical exposure, are given by the following differential equations, with the bulk solution in the delivery device being the control volume [16]:

$$\frac{dC_{NO}}{dt} = \frac{k_{NO}^{(NO)} A_{NO}}{V}\left[\alpha_{NO} P_{NO}^{(NO)} - C_{NO}\right] + \frac{k_{NO}^{(O_2)} A_{O_2}}{V}\left[\alpha_{NO} P_{NO}^{(O_2)} - C_{NO}\right] - 4k_1 C_{NO}^2 C_{O_2} \quad \text{(a)}$$

$$\frac{dC_{O_2}}{dt} = \frac{k_{O_2}^{(NO)} A_{NO}}{V}\left[\alpha_{O_2} P_{O_2}^{(NO)} - C_{O_2}\right] + \frac{k_{O_2}^{(O_2)} A_{O_2}}{V}\left[\alpha_{O_2} P_{O_2}^{(O_2)} - C_{O_2}\right] - k_1 C_{NO}^2 C_{O_2} \quad \text{(b)}$$

$$\frac{dC_{NO_2^-}}{dt} = \frac{A_{NOq}}{V} + 4k_1 C_{NO}^2 C_{O_2} \quad \text{(c)}$$

where $C_j$ is the time dependent concentration for species $j$, $A_{NO}$ and $A_{O_2}$ are the outer surface areas of the cylindrical tubing loops through which NO and $O_2$ are supplied, $V$ is the total liquid volume filling the device, $k_1$ is the rate constant from equation (4), $\alpha_j$ is the aqueous solubility for gas $j$, $k_j^{(i)}$ is the liquid phase mass transfer coefficient for gas $j$ inside the tubing supplying gas $i$, $P_j^{(i)}$ is the partial pressure of gas $j$ within the tubing loop supplying gas $i$, and $q$ is the extraneous flux of $NO_2^-$, a pseudo-heterogeneous reaction taking place in a micron thick layer next to the outer surface of the NO-supplying tubing loop (thought to be caused by intramembrane oxidation of NO to $NO_2$, with essentially all the produced $NO_2$ converted to $N_2O_3$ and subsequently to $NO_2^-$ at the interface [16]). The first two terms in the right hand side of Equations (a) and (b) represent mass transfer of the species in and out of the gas flows through the two tubing loops, whereas the third terms describe the net volumetric rates (consumption) of the dissolved gases in the bulk volume. The first term on the right hand side of Equation (c) represents the extra $NO_2^-$ source term added to the mass transfer model to account for the experimentally observed higher rate of $NO_2^-$ appearance during exposures, and the second term shows the rate of $NO_2^-$ formation from the reaction taking place in the bulk volume.

The system of equations can be simplified taking into account the following observations:

- cross contamination of NO from $O_2$, and vice versa, inside tubing loops can safely be assumed to be negligible, so $P_{NO}^{(O_2)} = P_{O_2}^{(NO)} = 0$
- NO loss through the tubing loop that supplies $O_2$, represented in Equation (a), is insignificant, since the term $\frac{k_{NO}^{(O_2)} A_{O_2}}{V} C_{NO}$ was shown to always be much smaller compared to the term $\frac{k_{NO}^{(NO)} A_{NO}}{V}\left[\alpha_{NO} P_{NO}^{(NO)} - C_{NO}\right]$ and thus can be ignored

altogether, eliminating the need to input a value for the mass transfer coefficient $k_{NO}^{(O_2)}$ in Equation (a)[16].

Using the mass transfer coefficients and physicochemical parameters displayed in Table 2, the dimensions of the delivery apparatus (filled with approximately 115 mL of fluid) and Silastic tubing loops (0.196 cm outer diameter), as well as experimentally determined pressure inside the tubing based on the given flow rates (~1.0 atm; ref. [16]) and initial values for the species concentrations at the beginning of each exposure ($O_2$ is the only species with non-zero initial concentration), the differential equations of the mass transfer model can be solved numerically to predict the time course of NO, $O_2$and $NO_2^-$ concentrations within the device employing MATLAB 7.11 (MathWorks, Natick, MA). Because of previous work that has shown strong effects of $O_2$ on the NO-related mass transfer coefficients and the conditions under which those values were estimated [16], it is important to use the model in cases where solutions and suspensions will be at nearly air-saturated levels to maximize the model's accuracy on predicting concentration profiles. To illustrate, Table 3 provides combinations of different tubing lengths and NO gas composition and the resulting calculated steady-state NO and $O_2$ levels expected to occur in the device during simulated exposures using water or buffers. As noted below, the model can also be used to validate and benchmark the operation of the system based on electrode measurements of NO and $O_2$.

### 2.7. Exposing cell cultures in the device

TK6 human lymphoblastoid cells [26,27] were obtained from ATCC, NH32 (an isogenic derivative of TK6; ref. [28]) and HCT116 human colon carcinoma cells [29,30] were provided by C. C. Harris (National Cancer Institute). TK6 and NH32 cells were kept in exponentially growing suspension cultures in RPMI-1640 medium supplemented with 10% heat-inactivated donor calf serum and HCT116 cells in McCoy's 5A medium supplemented with 10% heat-inactivated donor horse serum, at 37 °C in a humidified 5% $CO_2$ atmosphere; 100 units/mL penicillin, 100 μM/mL streptomycin and 2 mM L-glutamine were also added in both types of media. Cell suspensions were transferred at a density of $5 \times 10^5$ cells/mL in 115 mL of supplemented RPMI-1640 medium to sterile delivery devices (autoclaved at 120 °C for 20 min, with Silastic tubing loops of appropriate length already attached) immediately prior to treatment. Adherent cells were plated in 60 mm dishes ($10^6$ cells per dish) 24 h prior to exposure, existing medium was aspirated immediately before the exposure, and dishes were positioned at the bottom of autoclaved delivery devices (Supplementary Figure S2). The inner and outer surfaces of the dishes carrying the HCT116 cells needed to be sterile before insertion into the device, so handling was performed at all times with disinfected forceps within larger (150-mm) sterile dishes. Cell-carrying dishes without their caps were anchored for stability (using a small sterilized wedge made of Tygon tubing) to the bottom of the devices, and 110 mL of fresh supplemented McCoy's 5A medium were gently added immediately before the exposure begun. Tubing loops of suitable lengths and gas tanks of appropriate compositions were selected so that a steady state NO concentration of 0.6 μM was achieved in the case of cell suspensions and 1.8 μM in the case of adherent cells, with liquid $O_2$ levels maintained near air saturation. The total NO dose delivered was dictated by the exposure time and was quantified in units of μM min. Parallel exposures using Argon (instead of NO) were used as negative controls in all experiments. After the exposure, cell suspensions were collected by centrifugation and resuspended in fresh supplemented RPMI-1640 medium, whereas fresh supplemented McCoy's 5A medium was added to adherent cells cultures after being washed once with phosphate buffered saline. Subsequently, all cultures remained at 37 °C in a humidified 5% $CO_2$ atmosphere until further processing.

### 2.8. Cell viability analysis

TK6 and NH32 cell viability was determined 48 h after NO/$O_2$ treatment in the delivery device, whereas HCT116 cell viability was determined 24 h post exposure using the MTT assay (Roche Diagnostics, Indianapolis, IN) and following the manufacturer's instructions. Per cent survival was expressed relative to Argon-exposed negative controls at each treatment dose.

## 3. Results

### 3.1. Validation of NO and $O_2$ delivery in water

The basic operation of the system is illustrated with the simple scenario of NO and $O_2$ delivery into water in the absence of other chemical species that could react with NO or its derivatives. A modified delivery apparatus with NO and $O_2$ electrodes inserted through the vessel lid (Supplementary Figure S1) was used to measure dissolved gases in air-equilibrated de-ionized water. This allowed validation of the mass transfer model predictions of NO and $O_2$ steady-state levels achieved using the Silastic tubing of lengths, gas composition and gas flow conditions shown in Table 1. Measured levels of NO and $O_2$ in water agree well with model predictions at both 23 and 37 °C (Figure 2), with measured steady-state levels of 1.2 and 1.7 μM for NO and 240 and 210 μM for $O_2$, respectively.

The device can also be used to deliver predictable, well-controlled concentrations of NO-derived secondary species such as $NO_2^{\bullet}$ and $N_2O_3$. Though these species are too reactive to be measured directly, their mutual degradation product, $NO_2^-$, can be easily and accurately quantified [31]. Formation of $NO_2^-$ in the system operating with water deviated from the model's prediction by a factor of 1.6–2 (Figure 3), with correction for the model's extra $NO_2^-$ source $q$, ranging from 11 to 11.5 μmol $m^{-2}$ $s^{-1}$, providing a good fit of the data. (The origin of this extra $NO_2^-$ is discussed later.) This demonstrates the empirical nature of the mass transfer model and the need to calibrate the delivery system to account for batch-to-batch variations in Silastic tubing, which is important since there is a significant conversion of NO to $NO_2^{\bullet}$ within the tubing wall [22]. Table 4 summarizes optimized parameters for the model, estimated by minimizing sums of squared differences between measured and predicted concentrations of NO, $O_2$ and $NO_2^-$ at all time points (relative errors of concentration difference divided by measured concentration were used). Besides the $q$ values, the updated estimates of the mass transfer coefficients were in agreement with those previously reported (Table 2) [16].

The formation of $NO_2^-$ demonstrates an important factor in the operation of the delivery system. $NO_2^-$ generation is coupled with an equimolar accumulation of $H^+$, which necessitates the use of buffers to maintain a uniform pH within the device. For example, we observed that a solution of 50 mM phosphate buffer sustains a pH of 7.4 for over 12 h under the conditions defined in Figure 3 ($NO_2^-$ accumulation at 160 μM $hour^{-1}$), with accurate simulation of NO and $O_2$ levels by the mass transfer model [16,22]. Note that nitrate ($NO_3^-$) formation was not detected in previous studies [16] and was thus not measured here. The fact that model parameters describe levels of NO and $O_2$ equally well in water and phosphate buffers indicates that the presence of salts does not significantly affect delivery of NO or $O_2$ in the device.

### 3.2. NO and $O_2$ delivery in cell culture media

NO and $O_2$ delivery into cell culture systems presents a more complex scenario, with cell culture media typically containing nutrients and salts that could react with NO and its derivatives. For example, riboflavin in many media preparations has been shown to cause photo-induced generation of $O_2^{\cdot-}$ under standard lighting conditions [19,20]. The rapid

reaction of $O_2^{\cdot-}$ and NO to form $ONOO^-$ could thus act as a "sink" for NO and potentially interfere with the predicted steady-state NO concentrations in the device. We assessed this problem with two commonly used mammalian cell culture media: RPMI-1640 and Dulbecco's modified Eagle's medium (DMEM). The apparatus was filled with medium and delivery was initiated with the operational parameters used for water (Table 1). As shown in Figure 4A, the resulting concentration profiles for NO and $O_2$ in RPMI-1640 at both 23 and 37 °C were in good agreement with predictions from the mass transfer model. To assess the effects of riboflavin and ambient light on NO levels, the steady-state NO concentration was allowed to plateau in RPMI-1640 medium, at which point ambient lights were turned off (arrow in Figure 4A) to place the delivery device in complete darkness. As shown in Figure 4A, NO levels were identical in the presence or absence of ambient light, which ruled out substantial production of $O_2^{\cdot-}$ that would interfere with steady-state NO levels in RPMI-1640. Identical results were obtained with DMEM (Figure 4B), which contains twice the concentration of riboflavin as RPMI-1640 (1 vs. 0.5 μM, respectively). Consistent with the conclusion that the agreement observed between experimental measurements and model-generated curves is medium-independent, we observed that supplementation of RPMI medium with 10% heat-inactivated donor horse serum, 100 units/mL penicillin, 100 μg/mL streptomycin, and 2 mM L-glutamine also did not have an effect on the measured levels of NO at 37 °C, within the limits of accuracy of the electrodes (Supplementary Figure S5). It should be noted here that the vessel, connectors and Silastic tubing can be sterilized by autoclaving for work with cell cultures over prolonged periods, with minimal effect on performance. However, the system should be validated at least once following autoclaving to ensure that unique local conditions do not affect the NO and $O_2$ delivery parameters.

### 3.3. Exposure of cell cultures to NO and $O_2$

The full potential of the NO/$O_2$ delivery device is realized with exposure of cultured cells. As described above, the mass transfer model was used to determine exposure parameters (Silastic tubing lengths, gas composition) and calculate the steady-state gas levels before the device was used to generate the survival curves shown in Figure 5. Cultures of human lymphoblastoid TK6 cells and the p53-deficient derivative NH32 cells were then exposed to calculated levels of 0.64 μM NO and ~200 μM $O_2$ for up to 24 h, resulting in a cumulative total NO dose of 920 μM min and a dose-dependent pattern of cell death. Also evident in Figure 5, NH32 cells were relatively more resistant to NO toxicity than TK6 cells, with an apparent threshold for NO-induced cytotoxicity at ~300 μM min versus 150 μM min for TK6 cells. Interestingly, when either cell type was exposed to doses lower than its respective threshold, no significant cell death occurred [18]. The HCT116 adherent colon tumor cell line proved to be even more resistant to NO-induced cytotoxicity (Figure 5), with a threshold of ~1,000 μM min. That different killing curves were derived from widely used cell lines demonstrates the utility of the delivery device for studying mechanisms of NO function and toxicity. Exposure of control cell cultures to argon/$O_2$ had little or no effect on cell proliferation, which indicates minimal effects of turbulence caused by stirring in the reactor.

## DISCUSSION

There is an emerging recognition of the critical role of steady-state concentration in the biological function of NO and the enormous range of NO concentrations that distinguish physiological from pathological activity. However, most current NO delivery systems do not provide precise, accurate or long-term control of NO concentration [7,9]. Recent studies have led to interesting results, for example, on the response of an array of proteins to stratified levels of NO, with conclusions concerning anti- or pro-growth pathways related to the tumor microenvironment [11,32,33]. However, the means of NO delivery and estimation

of total NO dosage in those studies do not avoid the common caveats that accompany the use of NO-donor compounds. Further, typical extant NO delivery systems rely on the relatively hyperoxic conditions in aqueous solutions exposed to ambient air. We have overcome these limitations with a system to deliver well-controlled and biologically relevant steady-state concentrations of NO and $O_2$ to biomolecules and cells. The fact that $O_2$ is delivered separately from NO resolves the issue of depletion of the former through cellular respiration or its reaction with the latter, a technicality that affected previous attempts to develop a similar delivery system [25,34]. We have presented here a detailed step-by-step assembly and operation guide for the NO/$O_2$ delivery system, along with the means to validate the system. This provides the inexperienced user with sufficient information to fabricate the device from commercially available components, install it in a typical laboratory setting, and operate it safely and effectively. The system has broad utility in all types of in vitro studies of NO biology and chemistry, ranging from small molecule damage to exposures of suspension and mono-layer cell cultures to NO and its derivatives.

Based on our results, the mathematical model of mass transfer allows for accurate predictions of the NO and $O_2$ levels in both simple aqueous solutions and in cell media. By keeping steady operational parameters, such as gas flow-rates, stirring speed and temperature, and by varying NO composition (1%, 10% or 99% NO) and Silastic tubing loop length, the model computes the time-dependent NO, $O_2$ and $NO_2^-$ concentrations in the apparatus, provided that an experimental estimate of the initial $O_2$ concentration (before gas diffusion begins) is available. This can greatly facilitate experimental design, since changes in the configuration of the delivery apparatus (e.g., NO gas composition, tubing length) can be translated into predictable levels of NO, even before the actual gas delivery takes place. Further, the model allows fine-tuning of NO delivery by varying the lengths of the gas diffusion tubing.

The mass transfer model is readily modified to account for a variety of applications of the delivery device. For example, the initial formulation of the model assumed that cellular consumption of NO and $O_2$ would be negligible. Thus, all the predictions apply to cell-free culture media (or solutions) as was the case with some of the exposures presented here. However, recent studies revealed measurable rates of NO and $O_2$ consumption by several cell lines [17,20,35]. This allows a variation of the initial model in which the mass balance equation for each gas (differential equations delineating the net rate of change of NO and $O_2$ liquid concentrations, described in Section 2.6) includes an additional term representing the net specific cellular consumption rate for each gas multiplied by the cell density [17]. For instance, NO and $O_2$ consumption rates for TK6 cells (37 °C) were found to be 0.05 and 0.77 nmol $min^{-1}$ $(10^6 \text{ cells})^{-1}$, respectively, in a typical cell density of $5 \times 10^5$ cells $mL^{-1}$ (e.g., ref. [18]). By incorporating these new conditions into the model, we can predict changes in NO and $O_2$ concentrations caused by the cells (Supplementary Figure S6). Due to the order-of-magnitude difference in consumption rates, we observe a much less pronounced effect on NO concentration compared to $O_2$ levels, when computation extends from cell-free solutions to cell cultures. Consumption rates are available for a variety of cell lines, so employing accurate estimates of those terms in the model increases its predictive power. These kinds of customizations are relatively straightforward and add to the precision and accuracy of NO and $O_2$ delivery provided by the system.

The presence of nutrients in cell culture media such as salts, vitamins, amino acids, sugars, and glutathione did not measurably affect the diffusion of NO and $O_2$ through the Silastic membrane or their consumption in solution, with similar performance when gases were delivered in water. The lack of any molecular “sinks” for NO under normal lighting conditions or in a dark environment, even with serum-supplemented media, reinforces the expectation that the device will operate as predicted by the mass transfer model during

treatments of cell cultures. The lack of any apparent NO consumption when lights are activated in the vicinity of the device comes in contrast to previous studies [19,20] that attributed such trends to generation of $O_2^{\cdot-}$ presumed to originate from light-activated riboflavin in cell media. Although Keynes and coworkers did not describe their vessel characteristics in sufficient detail, Nalwaya and Deen used what was essentially a modified transparent polystyrene 60 mm culture dish to monitor reactions in media. On the other hand, the current delivery system is a semi-translucent 4 mm-thick Teflon container that may filter out wavelengths of laboratory light that could potentially excite riboflavin. Alternatively, $O_2^{\cdot-}$ formation inside the delivery device under the conditions describing the exposures may be smaller than the sensitivity of the probe that was used to measure NO levels.

The confidence that the mass transfer model gives in terms of steady delivery of NO and $O_2$ motivated a series of experiments to explore cellular responses to NO exposure [17,18,36,37]. Those studies revealed the existence of NO toxicity thresholds (sub-lethal vs. lethal) as well as repercussions in a diverse range of endpoints such as glutathione depletion, DNA damage, and cell growth arrest. This characteristic pattern of dose-dependent survival is likely to be true for all types of cells, offering opportunities for the device to be employed to monitor molecular damage and killing caused by NO, and to systematically study how sub-threshold NO affects cellular components and signaling pathways without simultaneously causing apoptosis or disturbing their growth cycle. The $NO/O_2$ delivery device is a versatile vessel that can accommodate cell cultures without itself affecting their survival. It is able to provide the gases of interest in a controllable and “clean” fashion, avoiding secondary effects that other delivery methods may cause.

A microscopic model developed to complement the general mass transfer model predicts that the apparatus has a 1 μm thick boundary layer adjacent to the NO tubing loop where the concentrations of oxidation intermediates $NO_2^{\bullet}$ and $N_2O_3$ greatly exceed those in the bulk liquid [22]. This “hot spot” appears to result from intramembrane oxidation of NO to $NO_2^{\bullet}$. The almost complete conversion of $NO_2^{\bullet}$ to $N_2O_3$ very close to the tubing surface explains the unexpectedly high rate of $N_2O_3$-derived $NO_2^-$ formation. Most molecules are small enough to enter the boundary layer and be exposed to high concentrations of $NO_2^{\bullet}$ and $N_2O_3$, which complicates the analysis when values of those concentrations are required for studies of chemical kinetics. An approach to estimate “hot spot” contributions to the total concentration compares reaction rates of target analytes to rates of another substrate with a known rate constant (e.g., morpholine nitrosation) [22,34,38]. However, the uncertainties introduced by this methodology motivated the development of a variation of the system in which NO is delivered through a porous Teflon membrane, instead of a Silastic tubing loop. Another modification is that the NO gas stream is fed through stainless steel (instead of Teflon) tubes, excluding any possible contamination by $O_2$ before oxidation takes place in the vessel [21]. The new design avoids adventitious $NO_2^-$ formation, so it is thought to eradicate the “hot spot” phenomenon. However, because the “hot spot” should not affect cells (10–20 mm diameter) due to their inability to enter the micron-thin boundary layer [22,39], and the Silastic-based apparatus is easier to fabricate and sterilize than the Teflon-based one, the Silastic apparatus remains the more attractive option for exposing cells.

As mentioned above, the extraneous $NO_2^-$ formation was postulated to be caused by intramembrane oxidation of NO to $NO_2^{\bullet}$. Previous work has reported a rate constant ($4.4 \times 10^5\ M^{-2}\ s^{-1}$) [16] for this conversion occurring within the Silastic tubing loop which was correlated to the rate at which $NO_2^-$ is formed in the bulk volume. Our results show a 1.6- to 2-fold increase in $NO_2^-$ accumulation during exposures to de-ionized water and a much smaller dependence on temperature (Fig. 3). In other words, if the intramembrane oxidation rate constant follows an Arrhenius-type behavior then our recent findings would point to a

greater pre-exponential factor and lower activation energy, perhaps due to variations in the physical properties of the Silastic tubing. Accordingly, it is advisable for a new user to validate the system and ascertain that the NO and $O_2$ delivery parameters are as expected. Alternatively, the observed increase of $NO_2^-$ formation could be related to incomplete exclusion of $O_2$ from the Teflon-based NO gas line as constructed in the current peripheral tubing system (noted by Skinn et al. [21]), which may differ from the original experimental setup that was used to determine the boundary layer contribution to $NO_2^-$ synthesis [16].

## Supplementary Material

Refer to Web version on PubMed Central for supplementary material.

## Acknowledgments

We gratefully acknowledge financial support from the National Cancer Institute (CA026731 and CA116318) and the National Institute of Environmental Health Sciences (ES002109), which supported quantitative studies in the Bioanalytical Facilities Core of the MIT Center for Environmental Health Sciences.

## REFERENCES

[1]. Moncada S, Palmer RM, Higgs EA. Pharmacol. Rev. 1991; 43:109. [PubMed: 1852778]

[2]. Thomas DD, Ridnour LA, Isenberg JS, Flores-Santana W, Switzer CH, Donzelli S, Hussain P, Vecoli C, Paolocci N, Ambs S, Colton CA, Harris CC, Roberts DD, Wink DA. Free Radic. Biol. Med. 2008; 45:18. [PubMed: 18439435]

[3]. Lim CH, Dedon PC, Deen WM. Chem. Res. Toxicol. 2008; 21:2134. [PubMed: 18828639]

[4]. Lewis RS, Tamir S, Tannenbaum SR, Deen WM. J. Biol. Chem. 1995; 270:29350. [PubMed: 7493969]

[5]. Dedon PC, Tannenbaum SR. Arch. Biochem. Biophys. 2004; 423:12. [PubMed: 14989259]

[6]. Coussens LM, Werb Z. Nature. 2002; 420:860. [PubMed: 12490959]

[7]. Keefer LK, Nims RW, Davies KM, Wink DA. Methods Enzymol. 1996; 268:281. [PubMed: 8782594]

[8]. Griffiths C, Wykes V, Bellamy TC, Garthwaite J. Mol. Pharm. 2003; 64:1349.

[9]. Schmidt, K.; Desch, W.; Klatt, P.; Kukovetz, WR.; Mayer, B. Nitric Oxide Protocols. Titheradge, MA., editor. Humana Press Inc.; Totowa, NJ: 1998. p. 281

[10]. Miranda KM, Katori T, Torres de Holding CL, Thomas L, Ridnour LA, McLendon WJ, Cologna SM, Dutton AS, Champion HC, Mancardi D, Tocchetti CG, Saavedra JE, Keefer LK, Houk KN, Fukuto JM, Kass DA, Paolocci N, Wink DA. J. Med. Chem. 2005; 48:8220. [PubMed: 16366603]

[11]. Thomas DD, Espey MG, Ridnour LA, Hofseth LJ, Mancardi D, Harris CC, Wink DA. Proc. Natl. Acad. Sci. USA. 2004; 101:8894–8899. [PubMed: 15178764]

[12]. Liu X, Miller MJ, Joshi MS, Thomas DD, Lancaster JR. Proc. Natl. Acad. Sci. USA. 1998; 95:2175. [PubMed: 9482858]

[13]. Pfeiffer S, Lass A, Schmidt K, Mayer B. FASEB J. 2001; 15:2355. [PubMed: 11689461]

[14]. Zhuang JC, Lin D, Lin C, Jethwaney D, Wogan GN. Free Radic. Biol. Med. 2002; 33:94. [PubMed: 12086687]

[15]. Lewis RS, Deen WM. Methods Enzymol. 1996; 268:247. [PubMed: 8782591]

[16]. Wang C, Deen WM. Ann. Biomed. Eng. 2003; 31:65. [PubMed: 12572657]

[17]. Wang C, Trudel LJ, Wogan GN, Deen WM. Chem. Res. Toxicol. 2003; 16:1004. [PubMed: 12924928]

[18]. Li C-Q, Pang B, Kiziltepe T, Trudel LJ, Engelward BP, Dedon PC, Wogan GN. Chem. Res. Toxicol. 2006; 19:399. [PubMed: 16544944]

[19]. Keynes RG, Griffiths C, Garthwaite J. Biochem. J. 2003; 369:399. [PubMed: 12366375]

[20]. Nalwaya N, Deen WM. Chem. Res. Toxicol. 2005; 18:486. [PubMed: 15777088]

[21]. Skinn BT, Lim CH, Deen WM. Free Radic. Biol. Med. 2011; 50:381. [PubMed: 21073946]

[22]. Dong M, Wang C, Deen WM, Dedon PC. Chem. Res. Toxicol. 2003; 16:1044. [PubMed: 12971791]

[23]. Schmidt, K.; Mayer, B. Nitric Oxide Protocols. Titheradge, MA., editor. Humana Press Inc.; Totowa, NJ: 1998. p. 101

[24]. Caulfield JL, Singh SP, Wishnok JS, Deen WM, Tannenbaum SR. J. Biol. Chem. 1996; 271:25859. [PubMed: 8824217]

[25]. Lewis RS, Deen WM. Chem. Res. Toxicol. 1994; 7:568. [PubMed: 7981422]

[26]. Levy JA, Virolain.M, Defendi V. Cancer. 1968; 22:517. [PubMed: 5673231]

[27]. Skopek TR, Liber HL, Penman BW, Thilly WG. Biochem. Biophys. Res. Commun. 1978; 84:411. [PubMed: 214074]

[28]. Chuang YYE, Chen Q, Liber HL. Cancer Res. 1999; 59:3073. [PubMed: 10397247]

[29]. Liu L, Taverna P, Whitacre CM, Chatterjee S, Gerson SL. Clin. Cancer Res. 1999; 5:2908. [PubMed: 10537360]

[30]. Hofseth, LJ.; Robles, AI.; Espey, MG.; Harris, CC. Nitric Oxide, Pt E. Elsevier Academic Press; San Diego: 2005. p. 326

[31]. Green LC, Wagner DA, Glogowski J, Skipper PL, Wishnok JS, Tannenbaum SR. Anal. Biochem. 1982; 126:131. [PubMed: 7181105]

[32]. Ridnour LA, Isenberg JS, Espey MG, Thomas DD, Roberts DD, Wink DA. Proc. Natl. Acad. Sci. USA. 2005; 102:13147. [PubMed: 16141331]

[33]. Ridnour LA, Thomas DD, Switzer C, Flores-Santana W, Isenberg JS, Ambs S, Roberts DD, Wink DA. Nitric Oxide-Biol. Chem. 2008; 19:73.

[34]. Caulfield JL, Wishnok JS, Tannenbaum SR. J. Biol. Chem. 1998; 273:12689. [PubMed: 9582291]

[35]. Chin MP, Schauer DB, Deen WM. Chem. Res. Toxicol. 2010; 23:778. [PubMed: 20201482]

[36]. Li CQ, Wright TL, Dong M, Dommels YEM, Trudel LJ, Dedon PC, Tannenbaum SR, Wogan GN. Free Radic. Biol. Med. 2005; 39:1489. [PubMed: 16274884]

[37]. Li CQ, Kim MY, Godoy LC, Thiantanawat A, Trudel LJ, Wogan GN. Proc. Natl. Acad. Sci. USA. 2009; 106:14547. [PubMed: 19706542]

[38]. Keshive M, Singh S, Wishnok JS, Tannenbaum SR, Deen WM. Chem. Res. Toxicol. 1996; 9:988. [PubMed: 8870986]

[39]. Dong M, Dedon PC. Chem. Res. Toxicol. 2006; 19:50. [PubMed: 16411656]

**Highlights**

- We developed a system for controlled delivery of biological relevant levels of NO and $O_2$.
- The fabrication, operation and calibration of the delivery system is described.
- The system was applied to deliver controlled steady-state NO and $O_2$ levels into cell culture media.
- Components of culture media do not to affect the steady-state levels of NO or $O_2$ in the device.

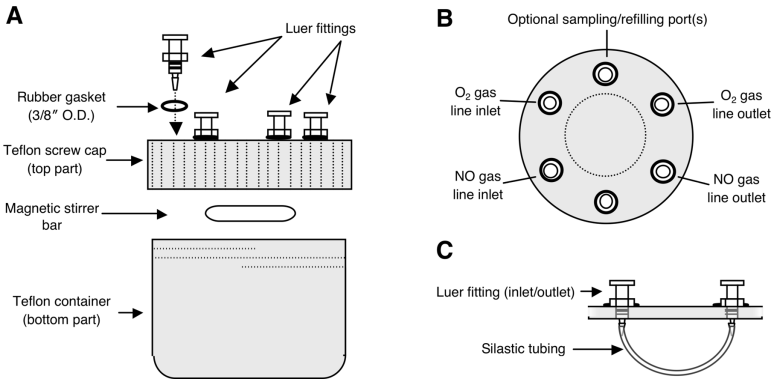


**Figure 1.**

Schematic of the $NO/O_2$ delivery apparatus. (**A**): Side view of the 120 mL Teflon container with hose-barb luer fittings threaded into holes in the screw cap with rubber gaskets to seal the connections. (**B**): Top view of the screw cap showing a typical arrangement of luer fittings and how they connect to external gas feeds. (**C**): Cross-section of the cap demonstrating connection of the U-shaped loop of Silastic tubing to two luer fittings for gas transit. All parts required to fabricate the apparatus are listed in Supplementary Table S2.

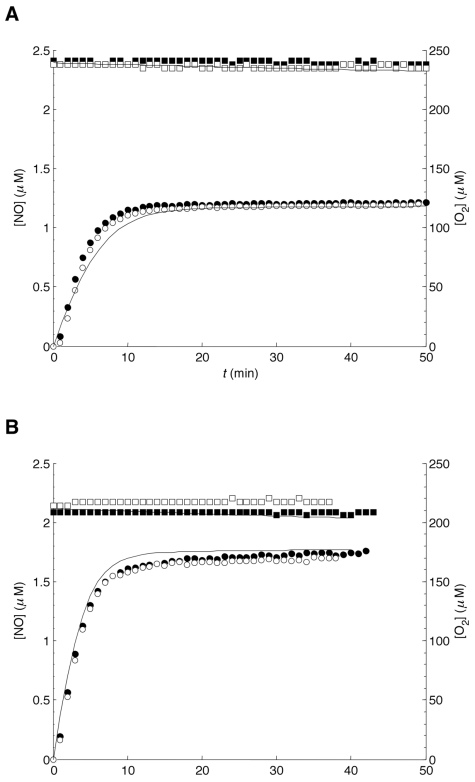


**Figure 2.**

Time course of measured and predicted bulk liquid NO (circles, left axis) and $O_2$ (squares, right axis) concentrations using water at 23 °C (**A**) and 37 °C (**B**). Data from two experiments (open and closed symbols) and predictions using the mass transfer model (solid curves) are shown. Exposure conditions: 10% NO, 100 sccm, 7.0 cm Silastic tubing loop; 50% $O_2$, 200 sccm, 5.3 cm tubing loop for 23 °C, or 6.3 cm tubing loop for 37 °C.

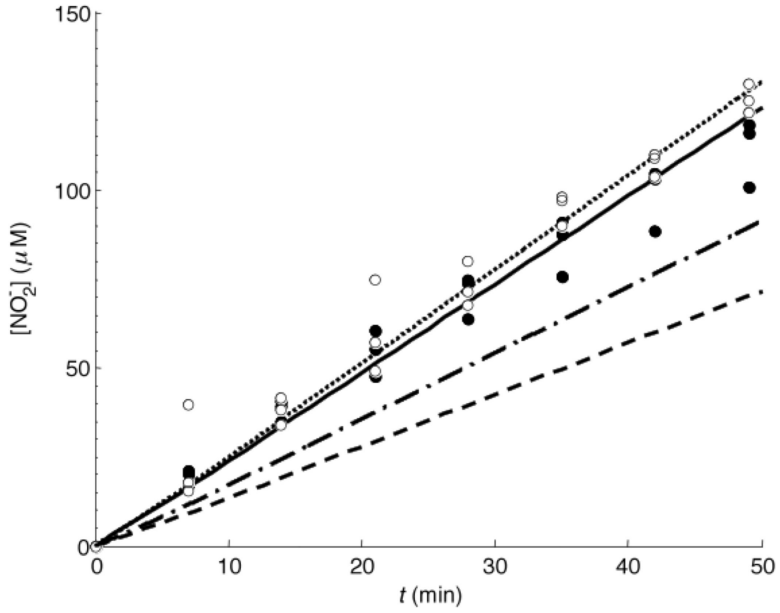


**Figure 3.**

Time course for measured and predicted nitrite ($NO_2^-$) formation. Discrete symbols represent experimental data (open circles from data at 37 °C, closed circles at 23 °C, triplicate measurements). The lines were generated by the mass transfer model: dotted line (37 °C) and solid line (23 °C) with $q$ = 11.03 and $q$ = 11.54 μmol $m^{-2}$ $s^{-1}$, respectively ($q$ values derived from recent data); dot-dashed line (37 °C) and dashed line (23 °C) with $q$ = 6.79 and $q$ = 5.70 μmol $m^{-2}$ $s^{-1}$, respectively (values from Table 2). Exposure conditions: 10% NO, 100 sccm, 7.0 cm Silastic tubing loop; 50% $O_2$, 200 sccm, 5.3 cm tubing loop for 23 °C, or 6.3 cm tubing loop for 37 °C.

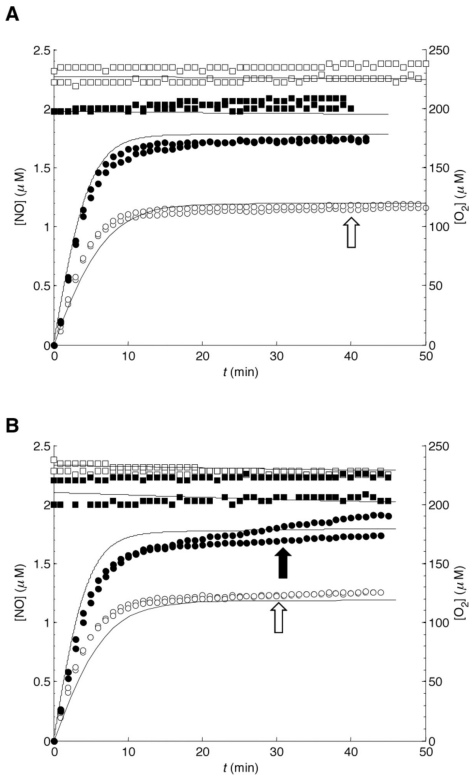


**Figure 4.**

Time course of measured and predicted bulk liquid NO (circles, left axis) and $O_2$ (squares, right axis) concentrations in **(A)** RPMI-1640 and **(B)** DMEM cell culture media at 23 °C (open symbols) or 37 °C (closed symbols). Data from two sets of experiments (discrete symbols) and predictions using the mass transfer model (solid curves) are shown. Arrows indicate the times at which ambient lighting was extinguished. Exposure conditions: 10% NO, 100 sccm, 7.0 cm Silastic tubing loop; 50% $O_2$, 200 sccm, 5.3 cm tubing loop for 23 °C, or 6.3 cm tubing loop for 37 °C.

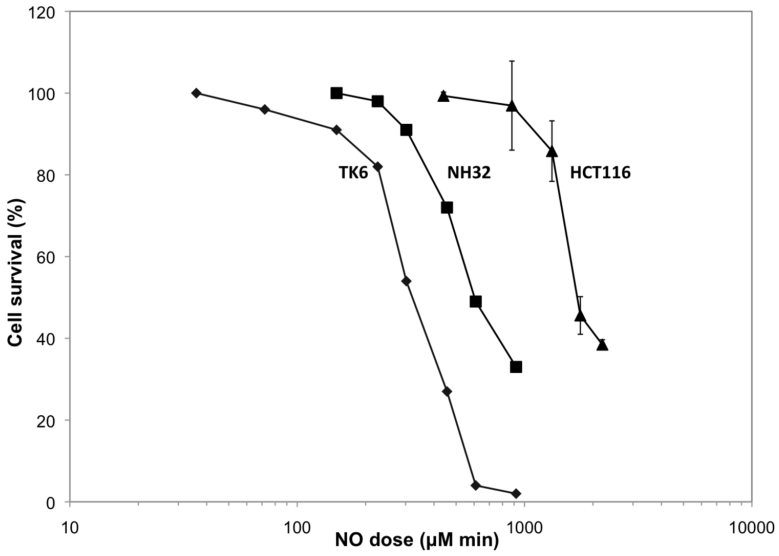


**Figure 5.**

Cell viability in TK6 and NH32 cells at 48 h and HCT116 cells at 24 h after exposure to NO and $O_2$ or argon at 37 °C. Cell viability was determined by MTT assay, as described in Materials and Methods. Data represent mean ± SD for 2–4 experiments; SD values for TK6 and NH32 cells were <8% and are not shown.

**Table 1**

NO and $O_2$ gas flow parameters for operation of the delivery system with water and culture media.

| | NO gas line | | | $O_2$ gas line | | |
|---|---|---|---|---|---|---|
| **Temp (°C)** | **Tubing length (cm)** | **Flow rate (sccm)** | **NO mole fraction (%)** | **Tubing length (cm)** | **Flow rate (sccm)** | **$O_2$ mole fraction (%)** |
| 23 | 7.0 | 100 | 10% | 5.3 | 200 | 50% |
| 37 | 7.0 | 100 | 10% | 6.3 | 200 | 50% |

**Table 2**

Input parameters for the mass transfer model.

| | 23 °C | | 37 °C | | |
|---|---|---|---|---|---|
| **Parameter** | **10% NO** | **99% NO** | **1% NO** | **10% NO** | **99% NO** |
| $k_{NO}^{(NO)}(10^{-5} m/s)$ | 0.40 | 1.07 | 2.06 | 1.11 | 1.84 |
| $k_{O_2}^{(NO)}(10^{-5} m/s)$ | 2.60 | 4.39 | 3.50 | 3.69 | 5.22 |
| $q$ (μmol m$^{-2}$ s$^{-1}$) | 5.70 | 33.8 | N.A. | 6.79 | 39.4 |
| $k_1$ (10$^6$ M$^{-2}$ s$^{-1}$) | 2.1 | | 2.4 | | |
| $k_{O_2}^{(NO)}(10^{-5} m\,s^{-1})$ | 2.01 | | 2.65 | | |
| $\alpha_{NO}$ (10$^{-8}$ M Pa$^{-1}$) | 1.8 | | 1.5 | | |
| $\alpha_{O_2}$ (10$^{-8}$ M Pa$^{-1}$) | 1.2 | | 1.0 | | |

*Symbols*: $k_{NO}^{(NO)}$, liquid phase mass transfer coefficient for NO and, $k_{O_2}^{(NO)}$, liquid phase mass transfer coefficient for $O_2$ at the tubing supplying NO; $q$, extraneous flux of $NO_2^-$ at the outer surface of the NO-supplying tubing loop; $k_1$, oxidation rate constant; $k_{O_2}^{(O_2)}$, liquid phase mass transfer coefficient for $O_2$ at the tubing supplying $O_2$; $\alpha_{NO}$, $\alpha_{O_2}$, aqueous solubility for NO, $O_2$, respectively. Values are reproduced from earlier studies [16,17]. No mass transfer coefficients available in the case of delivery of 1% NO at 23 °C.

**Table 3**

Predicted steady state NO and $O_2$ concentrations in simulated exposures.

| Temp. (°C) | Composition of NO stream | NO tubing length (cm) | $O_2$ tubing length (cm) | Steady-state [NO] (μM) | Steady-state [$O_2$] (μM) |
|---|---|---|---|---|---|
| 23 | 10% NO in Ar | 7.0 | 7.4 | 1.1 | 270 |
| | 99% NO | 5.0 | 12.3 | 4.8 | |
| 37 | 1% NO in Ar | 6.0 | 5.7 | 0.7 | 210 |
| | 10% NO in Ar | 7.0 | 7.3 | 1.8 | |
| | 99% NO | 5.0 | 11.5 | 6.0 | |

Composition of the $O_2$ stream is the same in every case (50% $O_2$ in $N_2$ with 5% $CO_2$). The $O_2$ concentration of the solution filling the apparatus before the start of every simulated exposure was arbitrarily selected to be that of air-saturated water (270 μM at 23 °C and 210 μM at 37 °C) and remained essentially stable during the simulation using the tubing length combinations displayed. Model parameters were not available for predictions in the case of 1% NO at 23 °C.

## Table 4

Mass transfer coefficients and boundary layer nitrite ($NO_2^-$) correction at the NO supplying tubing for operation of the delivery system with water.

| Temp (°C) | $k_{NO}^{(NO)}(10^{-5} m/s)$ | $k_{O_2}^{(NO)}(10^{-5} m/s)$ | $q$ (μmol $m^{-2}s^{-1}$) |
|---|---|---|---|
| 23 | 0.44 ± 0.03 | 2.3 ± 0.2 | 11.0 ± 0.95 |
| 37 | 1.0 ± 0.05 | 3.2 ± 0.35 | 11.5 ± 0.91 |

Updated mass transfer coefficients for NO, $O_2$ and boundary layer $NO_2^-$ source were based on data acquired with water (Figs. 2 and 3). Values for $k_{O_2}^{(O_2)}$ were taken from Table 2, assuming a negligible effect on $O_2$ delivery through the O2 supplying tubing at the NO concentrations used (ref. [16]).